Journal of Power Sources 236 (2013) 61–67

Contents lists available at SciVerse ScienceDirect

Journal of Power Sources

journal homepage: www.elsevier.com/locate/jpowsour

Lithium diffusion in sputter-deposited lithium iron phosphate thin-films

Mathias Köhler, Frank Berkemeier*, Tobias Gallasch, Guido Schmitz

Institut für Materialphysik, Universität Münster, Wilhelm-Klemm Str. 10, D-48149 Münster, Germany

HIGHLIGHTS

- ► LFP thin film electrodes are prepared by ion beam sputtering.
- ► Capacity and cycling stability show that the films are technically applicable.
- ► The films exhibit a strong texture in (210) and (311) direction.
- ► The lithium diffusivity of the films is found to agree to theoretical predictions.

ARTICLE INFO

Article history:
Received 26 November 2012
Received in revised form
1 February 2013
Accepted 14 February 2013
Available online 26 February 2013

Keywords:
Lithium ion battery
Thin film cathode
Lithium iron phosphate
Lithium diffusion
Sputter deposition

ABSTRACT

Thin films of lithium iron phosphate ($LiFePO_4$, LFP), with a thickness between 80 nm and 320 nm are prepared by ion beam sputter deposition. X-ray diffraction, transmission electron microscopy, and electron energy loss spectroscopy show that the films exhibit the desired structure, morphology, and chemical composition. Chrono potentiometry and cyclic voltammetry are carried out to determine the electrochemical behavior of the LFP films. Within these electrochemical measurements, a well-defined lithium intercalation/deintercalation reaction at around 3.45 V vs. Li/Li^+ and a specific capacity of 104 mAh g^{-1} are observed. Moreover, a quite high cycling stability is found: Measurement data at 1C rate indicate a capacity fading of only 20% after ≈1700 charge–discharge cycles. In addition, the diffusion of lithium within the LFP thin films is studied by cyclic voltammetry and galvanostatic intermittent transition technique. Within these measurements it is observed that the lithium kinetics in the sputter-deposited thin films is about two orders of magnitude faster, compared to the powder material and thin films deposited by pulsed laser deposition. This behavior may be explained by the strong texture of the sputtered films.

1. Introduction

Due to the increasing impact of lithium ion batteries, there is an intense demand on cheap, safe and environmentally compatible electrodes. Since lithium cobalt oxide, which is still one of the most common cathode materials, has deficits in either of these properties [1,2], there is an ongoing research for alternative cathode materials.

One of the promising candidates is lithium iron phosphate ($LiFePO_4$, LFP) which provides reliable safety, does not contain any toxic or expensive elements, and shows an excellent cycling stability [1,3,4]. It is well known that LFP exhibits an olivine-type structure with an orthorhombic unit cell (space group *Pmnb*) and a theoretical capacity of 170 mAh g^{-1} [1]. The uptake and release of lithium can be described by the reaction

$$LiFePO_4 \rightleftharpoons Li^+ + e^- + FePO_4.$$

Anyhow, electrochemical measurements on pure LFP powder result in a slightly lower experimental capacity of around 110 mAh g^{-1} (at 0.1 C) [5]. This discrepancy is usually explained by the quite low electronic and ionic conductivity of LFP [1,5].

In this work, we will report on the preparation of thin LFP films with a thickness between 80 nm and 320 nm by ion beam sputter deposition. Compared to conventional powder material, these thin films exhibit several outstanding features: On the one hand, they can be used for the preparation of lithium ion microbatteries. These types of batteries may significantly gain in importance in the near future [1,6,7] and require high-performance thin film electrodes that provide stable electrochemical properties, a dense structure, and an excellent surface quality. On the other hand, sputter-deposited thin films usually provide well-defined geometries and interfaces, and therefore represent excellent model systems to

* Corresponding author. Tel.: +49 (0) 251 833 677 0; fax: +49 (0) 251 833 834 6.
E-mail address: Frank.Berkemeier@uni-muenster.de (F. Berkemeier).

0378-7753/$ – see front matter © 2013 Elsevier B.V. All rights reserved.
http://dx.doi.org/10.1016/j.jpowsour.2013.02.043

fundamentally study e.g. the intercalation and deintercalation process or the formation of additional interface layers [2,8].

In the literature, there are some groups that report on the deposition of LFP thin films by pulsed laser deposition (PLD) [2,4,8,9]. Some of these films show quite reasonable electrochemical properties, but do not reach those of the powder material.

Only a few groups have investigated the preparation of LFP films by sputter deposition [10–12], although this technique provides significant advantages, since it can easily be assigned to different geometries and larger substrates. To our knowledge, all works done so far on sputter-deposited LFP films are dealing with films prepared by rf-magnetron sputter deposition [10–12]. Despite the prepared films show quite reasonable electrochemical properties, their capacities are still significantly lower compared to the powder material. Moreover, they exhibit a significant surface roughness which has to be regarded as a drawback when preparing complete thin film batteries. Furthermore, most of the works are discussing the co-deposition of LFP and carbon [10,11] or LFP and metallic components [12], respectively, and therefore do not provide fundamental information on the intrinsic properties of sputter-deposited LFP films.

In contrast, thin film samples prepared by ion beam sputtering do, in general, provide a well-defined morphology, high surface quality and a low surface roughness. Therefore, they can help to get further insight into the lithium kinetics in LFP, and may also be used as thin film cathodes in lithium ion microbatteries.

So, in the first part of this work, we study the structural, chemical, and electrochemical properties of ion beam sputtered LFP films by means of X-ray diffraction (XRD), transmission electron microscopy (TEM), chrono potentiometry, and cyclic voltammetry (CV). In the second part, we discuss the lithium diffusion in the thin films, measured by CV and the galvanostatic intermittent transition technique (GITT).

2. Experimental

2.1. Thin-film preparation

Thin films of LFP were prepared by ion beam sputter deposition [13]: Ar^+ ions, emitted by a 4 cm rf-source (Roth & Rau), are focused on a LFP target, exhibiting an energy of 0.9 keV and a current density of about 2.2 mA cm^{-2}. Consequently, target atoms are sputtered off from the target and deposited onto a substrate, forming a smooth and dense layer. The thickness of the layer is in-situ measured by a quartz crystal microbalance which was calibrated by TEM measurements. Since the whole deposition process is carried out under ultra high vacuum conditions ($\approx 10^{-8}$ mbar base pressure, $\approx 10^{-4}$ mbar working pressure), the influence of any kind of contamination can be neglected.

The LFP sputter target was prepared by cold pressing conventional, pure, uncoated LFP powder (EXM 1195, Südchemie [14]), resulting in a disk of 8 cm in diameter and 5 mm in thickness [13].

As substrates, polished semiconductor silicon wavers were used, with a lateral size of about 1 cm × 2 cm. Prior to layer deposition, the silicon was thermally oxidized at 1000 °C for 4 h, resulting in an amorphous SiO_2 layer of about 200 nm, which provides an electrical isolation between the silicon and the deposited thin films. Furthermore, a platinum layer of about 100 nm thickness was deposited between the SiO_2 and the LFP layer, serving as a current collector.

After deposition at room temperature, the thin films were encapsulated into a quartz glass tube filled with argon, and were annealed for 5 h between 400 °C and 650 °C, to obtain a crystalline structure.

2.2. Thin-film characterization

XRD, TEM, and EELS measurements were carried out to determine the morphology, crystal structure, and chemical composition of the LFP films.

The XRD spectra have been obtained using a *Kristalloflex D5000* (Siemens) in $\theta/2\theta$ Bragg-Brentano geometry and Cu-K_α radiation. For the TEM observations, a *LIBRA 200FE* (Zeiss) was used, equipped with an in-column omega energy filter, to measure the energy loss of the electrons while passing through the sample, and thus to obtain electron energy loss spectroscopy (EELS). The latter allows e.g. the determination of the ratio between phosphorous and iron, and to gain information about the layer stoichiometry. The preparation of the cross sections for the TEM investigations was done by conventional grinding, dimpling, and ion beam milling, described elsewhere [15].

To determine the electrochemical properties of the films, chrono potentiometry, cyclic voltammetry, and GITT measurements were carried out, using an *Ivium n-stat* (Ivium Technologies) galvanostat/potentiostat in a conventional three electrode configuration. Here, the sample served as the working electrode, while as counter and reference electrodes, pure lithium wire was used. During the electrochemical measurements, the electrodes were dipped into a liquid electrolyte (EC:DMC (1:1) containing 1 mol l^{-1} $LiClO_4$). The whole measurement cell was kept under inert atmosphere, using an argon-filled glovebox, to prevent any side reactions with e.g. oxygen or moisture.

3. Results and discussion

Since the electrochemical properties of the thin films are of significant interest, in a first step the storage capacities of 160 nm thin LFP films, annealed at different temperatures, were measured by CV between 3.0 V and 4.1 V vs. Li/Li^+ at a scan rate of 0.1 mV s^{-1}. The results of these measurements are shown in Fig. 1. In case of each sample, two peaks at around 3.5 V are observed, clearly indicating the intercalation and deintercalation reaction of lithium. Since no further peaks are observed, the presence of foreign phases that may react with lithium within this voltage window, can be excluded.

To calculate the volumetric intercalation capacity (negative current density) and deintercalation capacity (positive current density) of the films, the corresponding part of the CV curve is integrated and divided by the scan rate ν

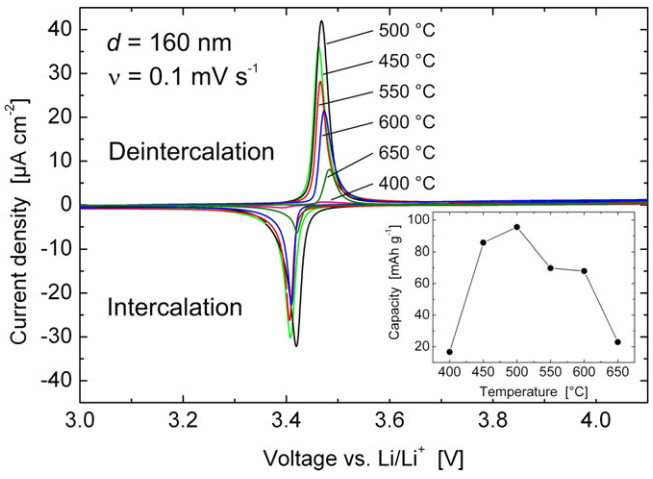

Fig. 1. CV data of 160 nm thin LFP films, annealed at different temperatures. The inset shows the capacity values as a function of the annealing temperature.

$$\kappa = \frac{1}{\nu} \cdot \int_{U_1}^{U_2} j(U)\mathrm{d}U, \quad (1)$$

where j is the current density and U the voltage. As shown in Fig. 1 (inset), it is obvious that samples annealed at 500 °C reveal the highest gravimetric capacity of 96 mAh g^{-1}. This behavior is in agreement with results obtained on LFP layers deposited by PLD, which also require post-annealing temperatures between 500 °C and 600 °C to reach their maximum capacity [8]. Since this temperature treatment at 500 °C under argon atmosphere results in maximum capacity values of the sputter-deposited films, all further LFP films in this work were prepared under these 'optimum' conditions.

3.1. Crystal structure and chemical composition

In a next step, the morphology of the deposited layers was checked. Using the stylus profilometer *DektakXT* (Bruker), the thickness of a LFP layer with a nominal thickness of 160 nm was found to be 164 ± 8 nm (Fig. 2), and thus demonstrates the reliability of the in-situ measurement by the quartz crystal microbalance.

To get more detailed information about the morphology of the films, TEM cross section micrographs were taken, as shown in Fig. 2. It is observed that the LFP film reveals a dense and crystalline structure, as well as a smooth surface. The same is valid for the platinum layer, but the interface between platinum and LFP appears quite rough, exhibiting a maximum roughness of about 15 nm. This interface roughness is due to the heat-treatment of the sample at 500 °C, which may cause an interdiffusion process between platinum and LFP, and thus results in a rough Pt-LFP reaction layer.

For further verification of the crystal structure, an XRD pattern of an optimum-prepared thin film is compared with those of the LFP powder material (Fig. 3). It is observed that beside the reflections of the silicon substrate and the platinum current collector, mainly three peaks of the LFP thin film are identified. These reflections correspond to the (210), (301), and (311) reflections of the LFP

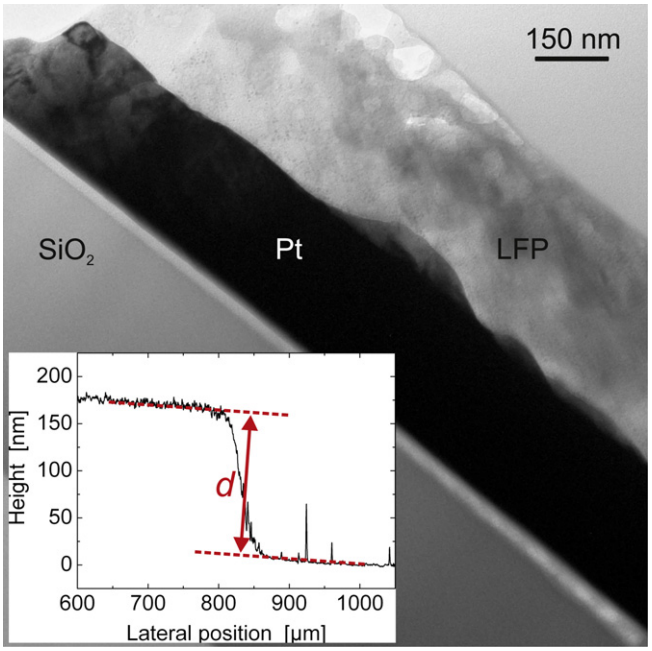

Fig. 2. TEM and profilometer measurements show the thickness, microstructure, and geometry of the films.

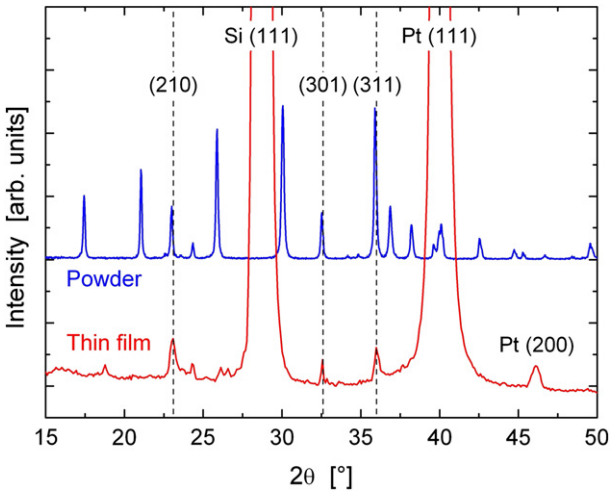

Fig. 3. XRD data of LFP powder material and a 250 nm thin LFP film.

powder and thus show that the deposited films reveal the designated, olivine-type crystal structure. However, it has to be noticed that they exhibit a quite pronounced texture, i.e. they show a strong orientation in [210], [301], and [311] direction, respectively.

To get detailed information about the chemical composition of the thin films, EELS spectra were obtained. As shown in Fig. 4, the absorption edges of all four elements (Li, P, O, Fe) can be identified within the spectrum, as well as the plasmon peak and the zero loss peak. Since the adsorption edge of lithium at around 55 eV is located within the range of plasmon excitation, a direct, quantitative evaluation of the lithium concentration is generally not possible by EELS. Anyhow, after deconvolution and background subtraction, the ratio of phosphorous and iron can be quantified to (0.77 ± 0.15), and therefore agrees within an error of 8% to the nominal one.

3.2. Specific capacity and cycling performance

After structure and composition have been verified, the electrochemical properties of the LFP films were studied in detail by means of chrono potentiometry, cyclic voltammetry, and GITT.

CV measurements were carried out on the LFP films, using a scan rate of 0.1 mV s^{-1}, as shown in Fig. 5 for the 1st, the 2nd, and the 18th CV cycle. As expected, clear reaction peaks (intercalation and

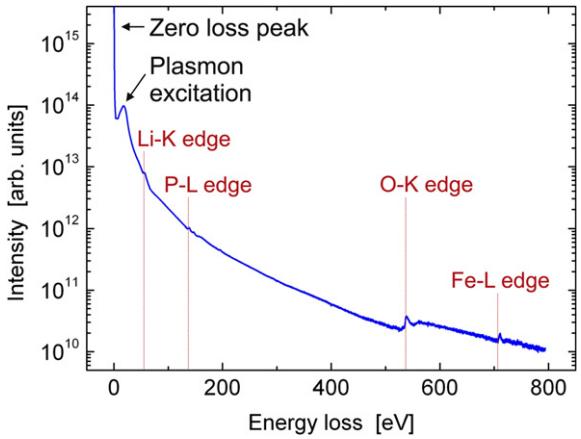

Fig. 4. EELS spectra of a LFP thin film. The zero-loss peak, the plasmon peak, and the absorption edges of Li, P, O, and Fe are observed.

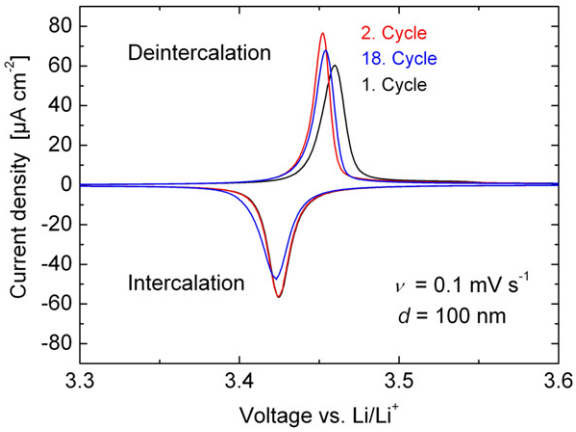

Fig. 5. CV data of a 100 nm thin LFP film, obtained at a scan rate of 0.1 mV s^{-1}. The 1st, 2nd, and 18th CV cycle are shown.

deintercalation) are observed. Between the 1st and the 2nd cycle, these peaks show a slight shift, but they remain approximately constant at 3.42 V (intercalation) and 3.45 V (deintercalation) between the 2nd and the 18th cycle.

The open cell voltage at the beginning of the measurements is found to be 3.16 V, indicating an initial state of charge of ≈100%, since the reaction peaks are located beyond this voltage value. The evaluation of the capacity proofs this assumption: Deintercalation capacities of 123.2 mAh g^{-1} (1st cycle), 110.0 mAh g^{-1} (2nd cycle), and 101.1 mAh g^{-1} (18th cycle) are found, which clearly indicates that the LFP films exhibit a lithium concentration after sputter deposition that is close to the maximum one.

To investigate the cycling stability of the films in more detail, chrono potentiometry measurements were carried out. At a current density of 10.4 µA cm^{-2} (which corresponds to a charge/discharge rate of about 1 C) a thin film sample underwent 210 cycles, while still revealing a remaining deintercalation capacity of ≈94% compared to the initial value (Fig. 6). It is also observed that the decrease in capacity shows a linear dependence on the cycle number n, between $n = 8$ and $n = 210$. Therefore, a linear extrapolation may be used to estimate the maximum cycle number until reaching a remaining capacity of 80%. This extrapolation results in about 1700 charge/discharge cycles, which is a quite reasonable value and further proves the assumption that the sputter-deposited films may be used in future all solid-state thin-film batteries.

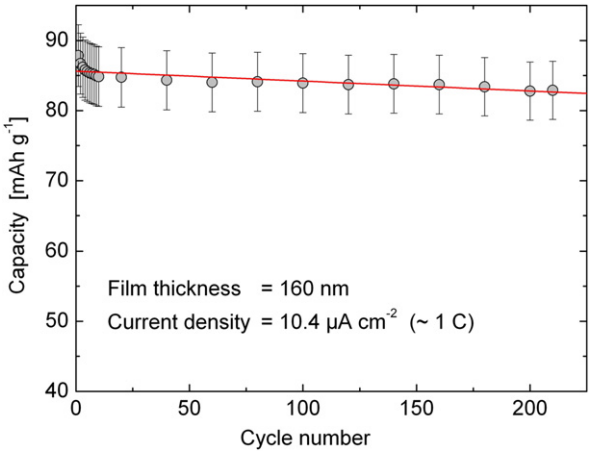

Fig. 6. Volumetric deintercalation capacity of a 160 nm thin LFP film as a function of the cycle number, measured by chrono potentiometry.

The chrono potentiometry measurements were also carried out at different current densities between 2 µA $cm^{-2}$and 42 µA cm^{-2}, while the thickness of the films denoted between 80 nm and 320 nm. The results of these measurements are given in Fig. 7. On the x-axis the volumetric capacity κ is given, calculated via

$$\kappa = \frac{j_0 \cdot (t_2 - t_1)}{d}, \tag{2}$$

where j_0 denotes the current density, t_1 and t_2 the start and end time of the measurement interval, and d the thickness of the layer. Negative capacities represent the deintercalation, while positive values represent the intercalation of lithium. In accordance with the clear intercalation and deintercalation peaks observed in the CV measurements (Fig. 5), all chrono potentiometry curves show a clear, well-defined voltage plateau among two divergent arms. Due to non-equilibrium conditions at higher charge/discharge rates, the capacity decreases with increasing current density.

If plotting the capacity per unit area versus the thickness of the layer, a linear relationship is observed, as shown in Fig. 7. The slope α of the regression lines is equivalent to the volumetric capacity κ of the LFP films, i.e. the capacity per unit volume. Via the mass density of LFP ($\rho_{LFP} = 3.5$ g cm^{-3} [18]), this value is transformed into the specific capacity, as summarized in Table 1.

It is observed that in case of the minimum applied current density of 2 µA cm^{-2}, a maximum specific capacity of about 104 mAh g^{-1} is measured. Depending on the thickness of the sample, this corresponds to a C-rate between 0.2 C and 0.7 C. In the case of uncoated powder materials, experimental values of 110 mAh g^{-1} (at 0.1 C) and 90 mAh g^{-1} (at 0.5 C) are reported in the literature [5]. Therefore, the capacities of the LPF films prepared in this work agree or even exceed the ones measured in case of the powder material, and thus the films may definitely be suitable for use in future technical applications.

In Fig. 7 it is also observed that the linear regression line does not cross the x-axis at $x = 0$, but at around 50 nm. This offset must be interpreted in such a way, that LFP films below ≈50 nm exhibit practical no lithium storage capacity. One possible explanation is the formation of an electrochemically inactive reaction layer. This layer can be interpreted as a solid electrolyte interface (SEI) at the top of the LFP films, but may also be an undesired reaction layer

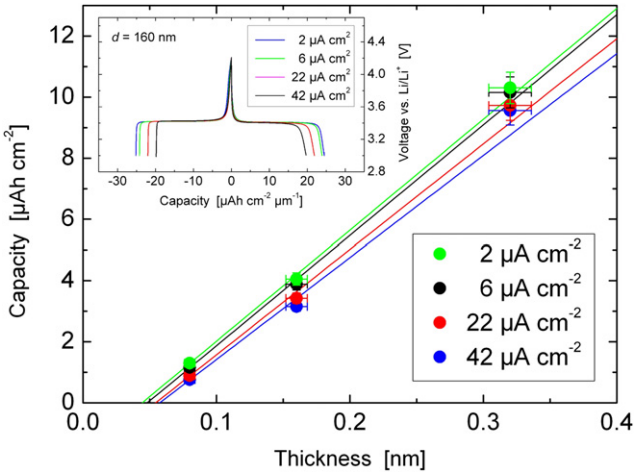

Fig. 7. Capacities of 160 nm thin LFP films, measured at different current densities. At each current density, a linear relationship between the capacity per unit area and the film thickness is observed. The intersection of the regression line and the x-axis is determined to be around 50 nm. As an inset, the chrono potentiometry data are shown.

Table 1
Capacities of the LFP thin films obtained from Fig. 7.

Current density [μA cm^{-2}]	Volumetric capacity [μAh cm^{-2} μm^{-1}]	Specific capacity [μAh g^{-1}]
2	36.3 ± 1.6	103.7 ± 4.6
6	36.1 ± 1.7	103.1 ± 4.9
22	34.5 ± 2.6	98.6 ± 7.4
42	33.4 ± 3.4	95.4 ± 9.7

between the platinum current collector and the LFP film, due to the necessary heat treatment of the samples at 500 °C. According to the data of Fig. 7, this inactive layer exhibits a thickness of around 50 nm and thus the 'electro-active' thickness of the deposited LFP is about 50 nm less compared to the nominal one.

3.3. Lithium diffusivity

The LFP films also represent a well-defined model system, to study fundamental properties and mechanisms of the intercalation and deintercalation process. Therefore, we studied the lithium diffusion within the films by means of CV and GITT.

To obtain diffusion data via CV measurements, CV curves were obtained at different scan rates, as shown in Fig. 8. According to Randles and Sevcik, the maximum current density j_p of the intercalation/deintercalation peak depends on the square root of the diffusion coefficient D [19,20]

$$j_p = 0.4463 \cdot zFc \cdot \sqrt{\frac{zF\nu D}{RT}}. \quad (3)$$

Here, z denotes the valency of the mobile ions, F Faraday's constant, c the concentration of mobile ions, R the universal gas constant, and T the absolute temperature. According to Eq. (3), plotting j_p as a function of $\sqrt{\nu}$ should result in a straight line with a slope proportional to $\sqrt{D}$. For the LFP thin films prepared in this work, such a Randles–Sevcik plot is shown in Fig. 9.

As expected, j_p depends linearly on $\sqrt{\nu}$ indicating a diffusion-controlled process. Therefore, the diffusivity of lithium is calculated for the intercalation and the deintercalation reaction, and is found to be

$$D^{int.} = (1.46 \pm 0.18) \cdot 10^{-13}\ cm^2\ s^{-1}$$
$$D^{de.} = (7.93 \pm 0.97) \cdot 10^{-14}\ cm^2\ s^{-1}.$$

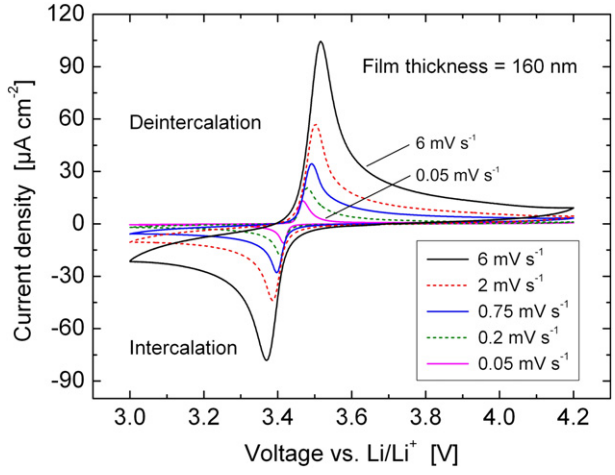

Fig. 8. CV data of a 160 nm thin LFP film as a function of the scan rate.

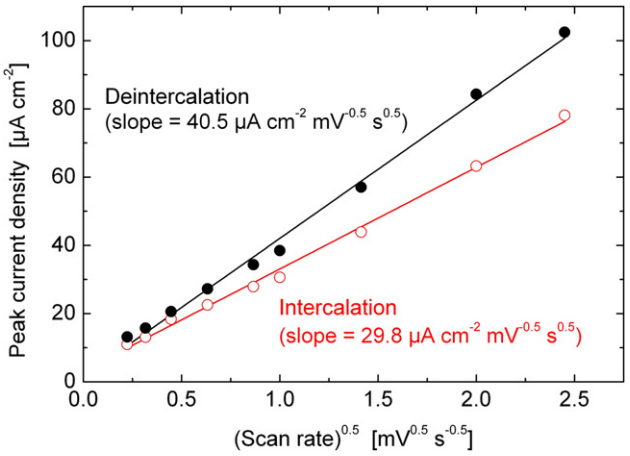

Fig. 9. Randles–Sevcik plot, obtained from the CV data of Fig. 8. Both, the intercalation and the deintercalation peak are evaluated.

However, the CV technique, in combination with the Randles–Sevcik plot, only allows to determine a concentration-averaged diffusion coefficient, but does not provide the possibility to measure the concentration dependence of D. Therefore, additionally, the more complex GITT technique [21] was also used to measure D.

In case of this technique, a constant current pulse is applied to the sample and the voltage characteristic is measured as a function of time [22]. Denoting U_0 the voltage of the sample vs. Li/Li$^+$ prior to the current pulse, U_p at the end of the pulse, and U_r after a sufficient relaxation time, according to Weppner et al. [21] the diffusion coefficient of the mobile species can be obtained via

$$D = \frac{4}{\pi\tau} \cdot \left(\frac{m \cdot V_M}{M \cdot A}\right)^2 \cdot \left(\frac{U_0 - U_r}{U_0 - U_p}\right)^2. \quad (4)$$

Here τ is the duration of the current pulse, m the mass of the electro-active material, M and V_M its molar mass and molar volume, respectively, and A is the surface area of the sample. Since

$$\frac{m \cdot V_M}{M \cdot A} = d,$$

with d as the layer thickness, it follows

$$D = \frac{4d^2}{\pi\tau} \cdot \left(\frac{U_0 - U_r}{U_0 - U_p}\right)^2. \quad (5)$$

Using GITT, in this work the lithium diffusion in a 160 nm thin LFP film was measured during the intercalation reaction as a function of the lithium concentration. For this purpose, the thin film sample was initially discharged (i.e. lithium was retracted) up to a voltage of 4.4 V vs. Li/Li$^+$, to guarantee a well-defined lithium concentration at the beginning of the measurement ($x = 0$ in Li_xFePO_4). Afterward, twelve similar GITT pulses were applied to the sample, resulting in a discrete charging of the thin film, until reaching the divergent arm of the voltage characteristic at around 3.2 V ($x = 1$ in Li_xFePO_4). Finally, the evaluation of each GITT pulse was used to determine the concentration-dependent diffusion coefficient of lithium within the LFP thin films.

In Fig. 10 the result of this measurement is plotted as a function of the lithium content. It is observed that the diffusivity of lithium varies between $3 \cdot 10^{-17}$ cm^2 s^{-1} and $3 \cdot 10^{-12}$ cm^2 s^{-1}, and reveals a minimum at around 60% lithium content. Qualitatively, this behavior has also been observed by Prosini et al. [23] in case of LFP

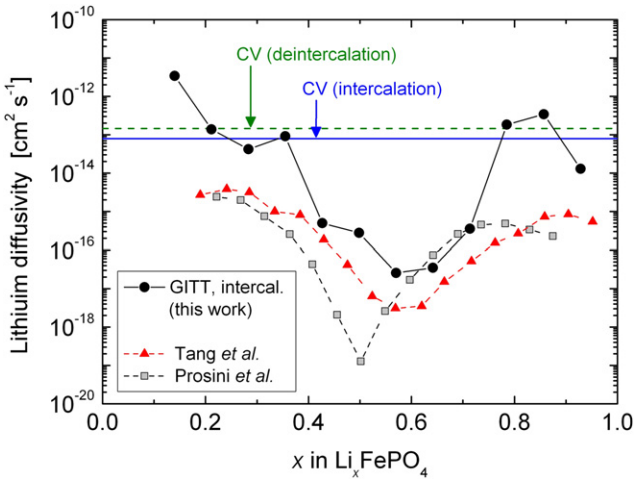

Fig. 10. Lithium diffusion data measured in this work compared to literature values reported by Tang et al. [9] and Prosini et al. [23].

powder material and by Tang et al. [9] in case of LFP thin films prepared by PLD. For comparison, these data of Prosini et al. and Tang et al. are also given in Fig. 10.

It's obvious that in case of all three measurements the lithium diffusivity exhibits a minimum at medium lithium concentrations. Anyhow, for further discussion, we will first consider the diffusion in case of lithium-poor and lithium-rich LFP, respectively, i.e. at $x < 0.4$ and at $x > 0.8$. In this case, it can be seen that the absolute values obtained in this work are about two orders of magnitude higher, compared to the values reported by Tang et al. and Prosini et al. Therefore, it seems reasonable to state that the thin films prepared by ion beam sputter deposition reveal an increased mobility, compared to LFP powder and to layers prepared by PLD, respectively.

This higher mobility of the sputter-deposited layers may be explained by different crystallographic properties: The LFP powder material is regarded to exhibit different crystallographic orientations, while the LFP films prepared by Tang et al. show a slight texture in [101] direction. In contrast to that, the XRD measurements of this work indicate that the films prepared by ion beam sputtering show a texture with preferred orientation in [210], [301] and [311] direction. Due to the fact, that the ionic motion in LFP is strongly anisotropic [24], this pronounced texture may increase the lithium kinetics within the films.

It is well known in the literature that the lithium ions within the LFP are located parallel to the *b*-axis of the orthorhombic unit cell [25], forming 1D 'diffusion channels' in the center of the cell. Therefore, the lithium atoms are expected to exhibit an increased mobility in *b* direction, and thus a decreased mobility in *a*- and *c*-direction [24]. Due to the fact that the films of Tang et al. exhibit a slight (101) texture, an unfavorable layer orientation may be concluded, since in that case the diffusion channels are oriented parallel to the sample surface. In contrast, the layers deposited in this work show a strong (210) and (311) texture, and thus the included angle between the diffusion channels and the substrate is significantly larger than 0°. This may lead to an increased kinetics of the lithium ions in case of the ion-beam sputtered thin films.

Moreover its worth to notice that the diffusivity values of the lithium-poor and lithium-rich LFP obtained in this work – which are found to be around 10^{-13} cm^2 s^{-1} – show a quite good agreement to the theoretical diffusivity values given by Zhu et al. [26] and Morgan et al. [24], who reported about lithium diffusivities in LFP between 10^{-12}–10^{-13} cm^2 s^{-1}.

Regarding the diffusivity minimum at $x \approx 0.6$ it has to be noted that the GITT method, which is used in this work to determine the lithium diffusivity, was originally derived for solid solutions, i.e. not for phase-separated materials [21,26]. Since the detailed atomic mechanism of intercalation and deintercalation of lithium in LFP is still discussed controversial [1], it's doubtful if solid solution conditions are applicable, or if instead e.g. some phase transition occurs during charging and discharging. There are various authors which argue that LFP undergoes a transition from lithium-poor α-phase to the lithium-rich β-phase (and vice versa) [3,27], which consequently would mean that the traditional GITT method can not be applied accurately, since it may cause deviations within the two phase region [26]. Hence, diffusivity values obtained at these medium concentrations need to be discussed, carefully.

Since a concentration averaged diffusion coefficient should be limited by minimum diffusivity values, the diffusivities measured by the CV method should also be around 10^{-17} cm^2 s^{-1}. As this is obviously not the case, this fact may also be regarded as an indicator that the diffusion in the lithium-rich and lithium-poor LFP films is in the range of 10^{-13} cm^2 s^{-1}, but that the diffusion data within the medium concentration range of $0.4 < x < 0.8$ obtained by GITT measurements are quite doubtful, due to the presence of a two-phase region.

4. Conclusions

In this work we studied the structural and electrochemical properties of ion beam sputtered LFP thin films. We proved the structure and stoichiometry of the films by XRD and analytical TEM, and observed that annealing of the as-prepared films at 500 °C under an argon atmosphere strongly improves their lithium storage capacity.

Detailed thickness dependent measurements of the capacity indicate that not the overall LFP layer is electrochemically active, but that there is an inactive region of about 50 nm in thickness, which may be caused by the heat treatment during the sample preparation at 500 °C. Taking into account this inactive part, a maximum capacity value of 104 mAh g^{-1} was found, which is clearly in the range of uncoated LFP powder. Moreover, the films show a quite satisfying cycling stability at 1 C-rate.

To our knowledge, LFP thin films of similar quality have not been reported in the literature, yet, and thus they strongly open the possibility to use them as cathode material in future thin film batteries.

Due to their well-defined geometry, the thin films were used to study the lithium kinetics within LFP. Within these measurements, a diffusion coefficient of around 10^{-13} cm^2 s^{-1} was found in case of lithium concentrations <40% and >80%. This quite high diffusivities are explained by the strong (210) and (311) texture of the films and are in good agreement with theoretical calculations by Zhu et al. and Morgan et al. However, at intermediate concentrations the diffusivity decreases down to 10^{-17} cm^2 s^{-1}. But since LFP may exhibit a two-phase region within this concentration range, these values need to be treated with care, as traditional GITT measurements can only be used accurately, in case of solid-solutions, but not in case of phase-separated materials.

Acknowledgment

The authors would like to thank the DFG for their financial support within the priority program 1473, as well as the BMBF for their founding within the project "LiVe" as part of innovation alliance "LIB 2015". Additionally, we would like to thank all members of the battery research center MEET in Münster for a plenty of fruitful discussions.

References

[1] Z. Li, D. Zhang, F. Yang, J. Mat. Sci. 44 (2009) 2435–2443.
[2] F. Sauvage, E. Baudrin, L. Gengembre, J.-M. Tarascon, Solid State Ionics 176 (2005) 1869–1876.
[3] A. Padhi, K. Nanjundaswamy, J. Goodenough, J. Electrochem. Soc. 144 (1997) 1188–1194.
[4] C. Legrand, L. Dupont, K. Tang, H. Li, X. Huang, E. Baudrin, Thin Solid Films 518 (2010) 5447–5451.
[5] Y. Dong, Y. Zhao, H. Duan, Mater. Chem. Phys. 129 (2011) 756–760.
[6] L. Hu, H. Wu, F. Mantia, Y. Yang, Y. Cui, ACS Nano 4 (2010) 5843–5848.
[7] J. Schwenzel, V. Thangadurain, W. Weppner, J. Power Sources 154 (2006) 232–238.
[8] C. Yada, Y. Iriyama, S.-K. Jeong, T. Abe, M. Inaba, Z. Ogumi, J. Power Sources 146 (2005) 559–564.
[9] K. Tang, X. Yu, J. Sun, H. Li, X. Huang, Electrochim. Acta 56 (2011).
[10] J. Hong, C. Wang, N. Dudney, M. Lance, J. Electrochem. Soc. 154 (2007) A805–A809.
[11] K. Chiu, J. Electrochem. Soc. 154 (2007) A129–A133.
[12] A. Eftekhari, J. Electrochem. Soc. 151 (2004) A1816–A1819.
[13] G. Schmitz, R. Abouzari, F. Berkemeier, T. Gallasch, G. Greiwe, T. Stockhoff, F. Wunde, Z. Phys. Chem. 224 (2010) 1795–1829.
[14] G. Nuspl, L. Wimmer, M. Eisgruber, Lithiummetallphosphate, Verfahren zu deren Herstellung und deren Verwendung als Elektrodenmaterialien, Patent specification, Süd-Chemie IP GmbH & Co. KG, 2004.
[15] A. Romano, J. Vanhellemont, H. Bender, J. Morante, Ultramicroscopy 31 (1989) 183–192.
[18] M. Gaberscek, R. Dominko, J. Jamnik, Electrochem. Commun. 9 (2007) 2778–2783.
[19] J. Randles, Trans. Faraday Soc. 44 (1948) 327–338.
[20] F. Lether, P. Wenston, Comput. Chem. 11 (1987) 179–183.
[21] R. Weppner, W. Huggins, J. Electrochem. Soc. 124 (1977) 1569–1578.
[22] F. Wunde, F. Berkemeier, G. Schmitz, J. Power Sources 215 (2012) 109–115.
[23] P. Prosini, M. Lisi, D. Zane, M. Pasquali, Solid State Ionics 148 (2002) 45–51.
[24] D. Morgan, A. Van der Ven, G. Ceder, Electrochem. Solid-State Lett. 7 (2004) A30–A32.
[25] T. Maxisch, G. Ceder, Phys. Rev. B 73 (2006) 174112.
[26] Y. Zhu, C. Wang, J. Phys. Chem. C 114 (2010) 2830–2841.
[27] C. Delmas, M. Maccario, L. Croguennec, F. Le Cras, F. Weill, Nat. Mater. 7 (2008) 665–671.